Atmospheric Research 181 (2016) 12–19

Contents lists available at ScienceDirect

Atmospheric Research

journal homepage: www.elsevier.com/locate/atmosres

Wavelength dependence of Ångström exponent and single scattering albedo observed by skyradiometer in Seoul, Korea

Ja-Ho Koo [a], Jhoon Kim [a,*], Jaehwa Lee [b,c], Thomas F. Eck [c], Yun Gon Lee [d], Sang Seo Park [a], Mijin Kim [a], Ukkyo Jung [a], Jongmin Yoon [e], Jungbin Mok [f], Hi-Ku Cho [a]

[a] Institute of Earth, Astronomy, and Atmosphere, Brain Korea 21 Program, Department of Atmospheric Sciences, Yonsei University, Seoul, Republic of Korea
[b] Earth System Science Interdisciplinary Center, University of Maryland, College Park, MD, USA
[c] NASA Goddard Space Flight Center, Greenbelt, MD, USA
[d] Research Institute of Basic Sciences, Chungnam National University, Daejeon, Republic of Korea
[e] Atmospheric Chemistry Department, Max-Planck Institute of Chemistry, P.O. Box 3060, 55020 Mainz, Germany
[f] Department of Atmospheric and Oceanic Sciences, University of Maryland, College Park, MD, USA

ARTICLE INFO

Article history:
Received 21 January 2016
Received in revised form 1 June 2016
Accepted 7 June 2016
Available online 08 June 2016

Keywords:
Aerosol
Skyradiometer
Ångström exponent
Single scattering albedo

ABSTRACT

Absorption and scattering characteristics of various aerosol events are investigated using 2-years of measurements from a skyradiometer at Yonsei University in Seoul, Korea. Both transported dust and anthropogenic aerosols are observed at distinct geo-location of Seoul, a megacity located a few thousand kilometers away from dust source regions in China. We focus on the wavelength dependence of Ångström exponent (AE) and single scattering albedo (SSA), showing the characteristics of regional aerosols. The correlation between spectral SSAs and AEs calculated using different wavelength pairs generally indicates relatively weak absorption of fine-mode aerosols (urban pollution and/or biomass burning) and strong absorption of coarse-mode aerosols (desert dust) at this location. AE ratio (AER), a ratio of AEs calculated using wavelength pair between shorter (340–675 nm) and longer wavelength pair (675–1020 nm) correlates differently with SSA according to the dominant size of local aerosols. Correlations between SSA and AER show strong absorption of aerosols for AER < 1.0 and weak absorption for AER > 2.0. Based on the seasonal pattern of wavelength dependence of AER and SSA, this correlation difference looks to reveal the separated characteristics of transported dust and anthropogenic particles from urban pollution respectively. The seasonal characteristics of AER and SSAs also show that the skyradiometer measurement with multiple wavelengths may be able to detect the water soluble brown carbon, one of the important secondary organic aerosols in the summertime atmospheric composition.

1. Introduction

It is well established now that the atmospheric aerosol is significantly playing an important role in global climate changes (e.g. IPCC, 2013). There have been numerous studies to evaluate the characteristics of aerosols, which however still include large uncertainty for both direct (e.g., Charson et al., 1992) and indirect effect (e.g., Rosenfeld, 2000). Ground-based network such as AErosol RObotic NETwork (AERONET) (e.g., Holben et al., 1998), SKYradiometer NETwork (SKYNET) (e.g., Boi et al., 1999), and Chinese Sun Hazemeter Network (CSHNET) (e.g., Xin et al., 2007) have deployed sunphotometers and skyradiometers for the long-term observation of aerosol in the global scale. These networks have provided various parameters at multiple wavelengths to monitor column integrated aerosol optical properties. Several previous studies found that these ground-based measurements of aerosol optical properties show large sensitivity to the selected wavelengths (Eck et al., 1999, 2003, 2005, 2008). Namely, the size and composition of the aerosol, which eventually lead to uncertainties in evaluating radiative forcing, can be estimated based on the wavelength dependence of aerosol optical properties. In addition to evaluating climatic influences of aerosols, the analysis of wavelength dependence will be also useful to better understand spatiotemporal characteristics of regional aerosol properties (Kim et al., 2007a, 2007b; Lee et al., 2010a, 2010b; Masmoudi et al., 2015).

There have been many studies to investigate the wavelength dependence in optical measurements of aerosol, mostly based on the aerosol optical depth (AOD) and its wavelength dependence called Ångström Exponent (AE). Cachorro et al. (1987) recognized the variation of AOD with respect to wavelengths and verified the method to determine Ångström turbidity. Kaufman (1993) found that AE providing the size information of atmospheric aerosol becomes different according to the selected wavelength pairs. The wavelength dependence of AE values seems to show regional difference (Kaskaoutis and Kambezidis, 2006;

* Corresponding author.
E-mail address: jkim2@yonsei.ac.kr (J. Kim).

http://dx.doi.org/10.1016/j.atmosres.2016.06.006
0169-8095/

Ningombam et al., 2015) and seasonal variation (Ganguly et al., 2006), and also to reveal correlations with the size information of aerosol such as the volume fraction and the effective radius (Schuster et al., 2006). Moreover, the wavelength dependence of AEs results in the curved relationship between AOD and wavelength in logarithmic coordinates, and several studies indicated that this curvature shape reflects the dominant type of the regional aerosol (Eck et al., 1999; Kaskaoutis and Kambezidis, 2006).

The single scattering albedo (SSA hereafter) shows the extent of scattering due to the atmospheric aerosol. SSA varies significantly with respect to the measured wavelength (Dubovik et al., 1998; Eck et al., 2003; Lee et al., 2007; Alam et al., 2011) because the scattering efficiency changes strongly in accordance with the refractive indices, which has the wavelength dependence. Dubovik et al. (2002) and Russell et al. (2010) analyzed the variation of SSAs for different wavelengths at several representative regions to show the regional difference of dominant aerosols. Eck et al. (2005) and Eck et al. (2008) analyzed local aerosol properties based on the information of wavelength dependence of SSAs. Eck et al. (2010) performed a deeper investigation and revealed some advanced findings about the spectral variation of SSA according to the mixing between fine and coarse mode particles. Li et al. (2015) recently estimated the SSA spectral curvature to infer how much different aerosol types are mixed.

Based on these previous findings, this study focuses on the aerosol properties in Seoul, a representative megacity under both the influence of Asian dusts and anthropogenic pollution (e.g., Guo et al., 2010). The observation of aerosol properties in Seoul was started using multiple-channel Volz spectrophotometer (Volz 529) since 1980s. Cho (1980) first attempted to find the wavelength dependence of aerosol extinction and particle size distribution in Seoul. Cho (1981) also found that Ångström turbidity coefficients appear differently according to the wavelength selected. Cho et al. (1984) tried to analyze Ångström's power law and how this wavelength dependence looks like according to the different condition of turbidity. These studies have shown interesting results such as the change of diffuse ratio of incoming solar radiation at various channels. As ground-based networks such as AERONET or SKYNET have expanded, it has continued to monitor aerosol optical properties in Seoul and also in many other sites of East Asia. Some of previous studies found the peculiar characteristics such as the peak of AOD in June (Kim et al., 2007a, 2007b), large SSA over the desert area (Kim et al., 2004a, 2004b; Kim et al., 2005), and so on. However, studies for the wavelength dependence of aerosol optical properties have not been examined much in Seoul and East Asia area.

This study mainly investigated the aerosol characteristics in more systematic ways with skyradiometer measurements at Seoul operated since 2005. In particular, this study focused on the wavelength dependence of SSA and AE. All results provided in this study will be useful for the estimation of the variation of regional radiative forcing and classification of the type of regional aerosols.

2. Data description

The skyradiometer (model POM-02, Prede Co. Ltd.) is a ground-based instrument, measuring the direct and diffuse solar radiance to retrieve aerosol optical parameters at 11 channels (315, 340, 380, 400, 500, 675, 870, 940, 1020, 1600, 2200 nm) for every 10 min. The skyradiometer has two observation geometries, which are principal and almucantar methods. Principal method observes the solar radiance with varying zenith angle at fixed azimuth angle, and almucantar measures with varying azimuth angle at fixed zenith angle (Aoki and Fujiyoshi, 2003). Raw data measured by these two methods are processed using the radiative model package, Skyrad.pack version 4.2 (Nakajima et al., 1996; Takamura and Nakajima, 2004) to retrieve physical parameters of aerosol optical properties such as AOD, SSA and volume size distribution. Skyrad.pack includes the kernel function for extinction and scattering of aerosol from the Mie code. Then aerosol optical properties are retrieved from the inversion process (Nakajima et al., 1996) using the diffuse sky flux normalized by the direct flux. More details for the inversion process are described in Nakajima et al. (1996) and Boi et al. (1999).

In 2005, a POM-02 skyradiometer was installed at Yonsei University (37.57°N, 126.97°E) in Seoul, South Korea (see supplement materials), to monitor the aerosol optical properties in Seoul. In this study, two-year measurements from the skyradiometer were used (from December 2005 to November 2007). We used AODs and SSAs measured at 7 channels (340, 380, 400, 500, 675, 870, 1020 nm), and AEs calculated from AODs at six different pairs of neighboring wavelengths. All data were basically qualified by iteration processes in Skyrad.pack and verification, such as removing extreme values (i.e. lower than 5th percentile and higher than 95th percentiles of each parameter). Cloud screening process is one of important processes in data verification. For the optical measurement by AERONET sunphotometer, cloud screening process is usually based on the algorithm of Smirnov et al. (2000). While this algorithm was already verified in many previous studies and is still widely used, this screening method is not exactly applied to the current work because the criteria index D in the algorithm (Smirnov et al., 2000) needs to be tuned for different instrumentation. Therefore SKYNET developed another cloud screening algorithm for skyradiometer measurements (Khatri and Takamura, 2009; Song et al., 2014). Skyradiometer basically stops its measurement when the sun sensor detects the cloud interference. To remove the data perturbed by the cloud, we also delete 3% of data showing the highest standard deviation among continuous five measurements. Finally, data in March and December of 2006, and July and September of 2007 were not used due to the poor quality from bad weather condition and/or instrumental problems. The total number of available daily mean data is 250 in 2006 and 223 in 2007 as listed in Table 1.

Before analyzing data, several factors were carefully deliberated regarding the range of bias. First question is about the feasibility to use the UV measurements for aerosol optical analysis. Previously UV channel was not used much due to the influence of absorption by ozone and other trace gases (e.g., SO_2), but recently several UV channels were selected for the aerosol optical measurements. For example, 340 and 380 nm is used in the sunphotometer or skyradiometer and even shorter channel 320.1 nm can be used for AOD retrieval in the Brewer spectrophotometer (Kerr, 2002). Several studies verified the quality of AOD measured in these UV-channels by the inter-comparison among different instruments (Cheymol et al., 2009; De Bock et al., 2010). For this study, AOD from UV channel measurements of skyradiometer was also verified with the data measured in the 320.1 nm of Brewer spectrophotometer located in the same site (Koo, 2008). The quality of skyradiometer measurement itself is another factor to be considered. Compared to the CIMEL sunphotometer used in the AERONET, skyradiometer measurements of the SKYNET tend to overestimate the peak of coarse mode (Che et al., 2008). But Estellés et al. (2012a) mentioned that aerosol volume distribution obtained from SKYNET becomes comparable with that from AERONET when AOD is high. Actually inter-comparison shows that the retrieved aerosol optical properties are generally comparable between the two different instrumental measurements (Estellés et al., 2012a, 2012b). Also AODs measured by skyradiometer at Seoul were verified with AODs from Multi-Filter Rotating Shadowband Radiometer (MFRSR) retrieved by the Langley method (Cho et al., 2003; Koo, 2008). Therefore, it can be assumed that quality of data used in this study is reasonably guaranteed.

3. Results and analysis

First, general characteristics of aerosol optical properties are examined in Seoul. Table 1 shows the seasonal mean AODs (500 nm), SSAs (500 nm), and AEs (400–675 nm) from December 2005 to November 2007. This table shows the overall status of aerosol loading in Seoul. AOD is large in spring and summer, and relatively low from mid-

Table 1
Seasonal mean values of AOD, SSA, and AE from December 2005 to November 2007. March 2006, December 2006, July 2007, and September 2007 were not considered in this study due to the poor measurements affected by bad weather conditions and instrumental problems.

Year	The number of daily data		AOD (500 nm)		SSA (500 nm)		AE (400–675 nm)	
	2005–2006	2006–2007	2005–2006	2006–2007	2005–2006	2006–2007	2005–2006	2006–2007
DJF	73	53	0.433	0.564	0.921	0.927	1.003	0.969
MAM	39	80	0.834	0.816	0.904	0.915	0.818	0.898
JJA	60	40	1.045	0.755	0.932	0.925	0.879	0.808
SON	78	50	0.604	0.466	0.926	0.929	0.992	1.114

autumn to mid-winter. AOD is sometimes highly enhanced in early summer before rainy season in Korea because the air condition at this time is typically quite stagnant and humid, preferred condition for the high aerosol loading and growing. This atmospheric condition seems suitable for the strong hygroscopic growth of particle (Kim et al., 2007a, 2007b; Koo, 2008). SSA and AE show similar seasonal patterns, which is small in spring (more absorbing by large particle) and large in winter (more scattering by small particle). All these parameters generally show the distinctive pattern of springtime Asian dust and hygroscopic growth of summertime aerosols in Seoul (Koo, 2008; Huang et al., 2015).

3.1. Wavelength dependence based on correlations between SSA and AE

The variation of scattering efficiency corresponding to the wavelength is dependent on the particle size, shape, and composition according to the Mie theory (Liou, 2002). This is the basic reason that AE differs as the wavelength interval changes (Reid et al., 1999; Ganguly et al., 2006). To look into this aspect more, correlations of 500 nm SSAs were calculated with AEs from different wavelength pairs (Supplementary material). AEs were obtained at six wavelength intervals which are 340–380 nm (AE1), 380–400 nm (AE2), 400–500 nm (AE3), 500–675 nm (AE4), 675–870 nm (AE5), and 870–1020 nm (AE6). It is interesting to note that SSA reveals stronger positive correlation with AEs from longer wavelength pair (r^2 reaches up to 0.818). In other words, the line of linear least square fit turns counterclockwise as a wavelength pair of AE moves to longer part of the spectrum (Fig. 1).

The wavelength dependence of correlations between SSAs and AEs are also investigated in accordance with the size of aerosol. It is known that AEs calculated in the visible spectrum range generally show largely positive correlation with the fine mode fraction of aerosols: small AE representing coarse-mode dominance and vice versa (e.g., Wang et al., 2011). Thus, fine mode and coarse mode dominant cases are divided using AEs at 400–675 nm (Liu et al., 2008; El-Metwally and Alfaro, 2013). Fig. 1 presents correlations between SSAs and AEs for three different cases, which are total (Fig. 1a), fine mode dominant (AE at 400–675 nm > 0.75, Fig. 1b), and coarse mode dominant (AE at 400–675 nm < 0.75, Fig. 1c) cases (e.g., Ningombam et al., 2014). Comparing the correlation between SSA and AE for the fine and coarse mode dominant cases separately, it was clearly noticed that SSAs at 500 nm were negatively correlated with AE at shorter wavelength pairs (SW-AE), and positively correlated with AE at longer wavelength pairs (LW-AE) (Fig. 1b and c). But for the total case, negative correlations between SSA and SW-AEs were not clearly shown (Fig. 1a).

In addition to AEs with different wavelength intervals, SSAs for other different wavelengths (340, 380, 400, 500, 675, 870, and 1020 nm) were also used for the correlation analysis in a same way as in Fig. 1. Then we summarized the slope and r^2 of the linear regression between SSA at all seven channels and six AEs for three particle size cases (total, fine-mode, and coarse-mode dominant case) (Fig. 2). The extent of correlations is varied according to not only the different wavelength pairs of AEs, but also the wavelength of SSA. In detail, SSA is negatively correlated with SW-AEs (AE1 and AE2) and positively with LW-AEs (AE4, AE5, and AE6). This pattern is shown more distinctive in each case of fine or coarse mode dominance, not in the total case. Positive correlations between SSA and LW-AE generally seem to be stronger than negative correlations between SSA and SW-AE. Correlations between SSA and SW-AE becomes a little high in the coarse-mode dominant case (Fig. 2f). Interestingly, SSA at longer wavelengths (LW-SSA) shows large r^2 with SW-AE, but SSA at shorter wavelengths (SW-SSA) shows large r^2 with LW-AE.

All the wavelength-dependent patterns about the relationship of SSAs and AEs are summarized as follows:

1. SSA at wavelength of 500 nm correlates negatively with SW-AE, but positively with LW-AE.
2. The extent of correlation of SSA is weak (small r^2) with SW-AE, but strong (large r^2) with LW-AE.
3. LW-AE shows the larger positive correlation with SW-SSA, while SW-AE shows better correlation with LW-SSA.

These characteristics between SSA and AE show the complex pattern of wavelength dependence of aerosol optical properties. As widely

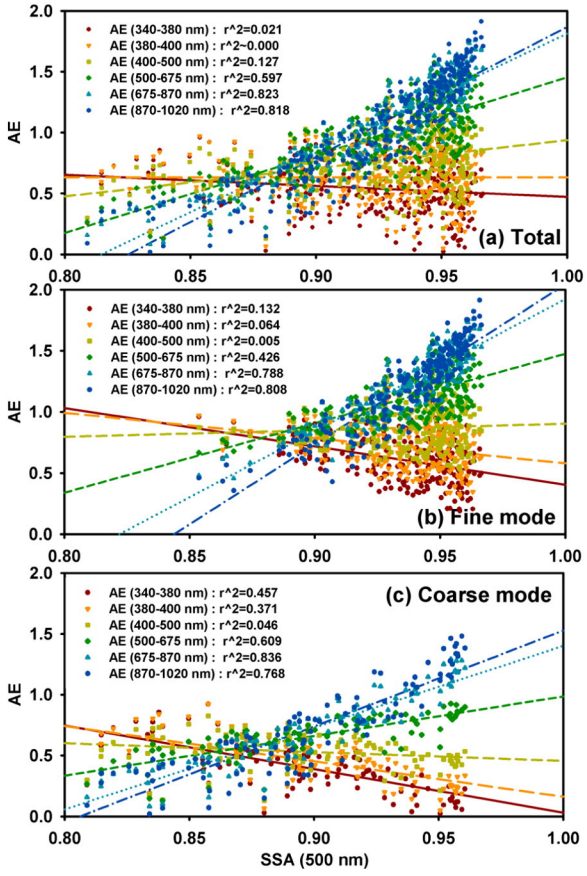

Fig. 1. Correlations of single scattering albedo (SSA) at 500 nm with Ångström exponent (AE) at 6 wavelength pairs such as 340–380 (red), 380–400 (orange), 400–500 (yellow green), 500–675 (green), 675–870 (cyan), and 870–1020 (blue dots) nm for three different conditions, which are (a) totally ambient, (b) fine mode dominant, and (c) coarse mode dominant conditions. (For interpretation of the references to color in this figure legend, the reader is referred to the web version of this article.)

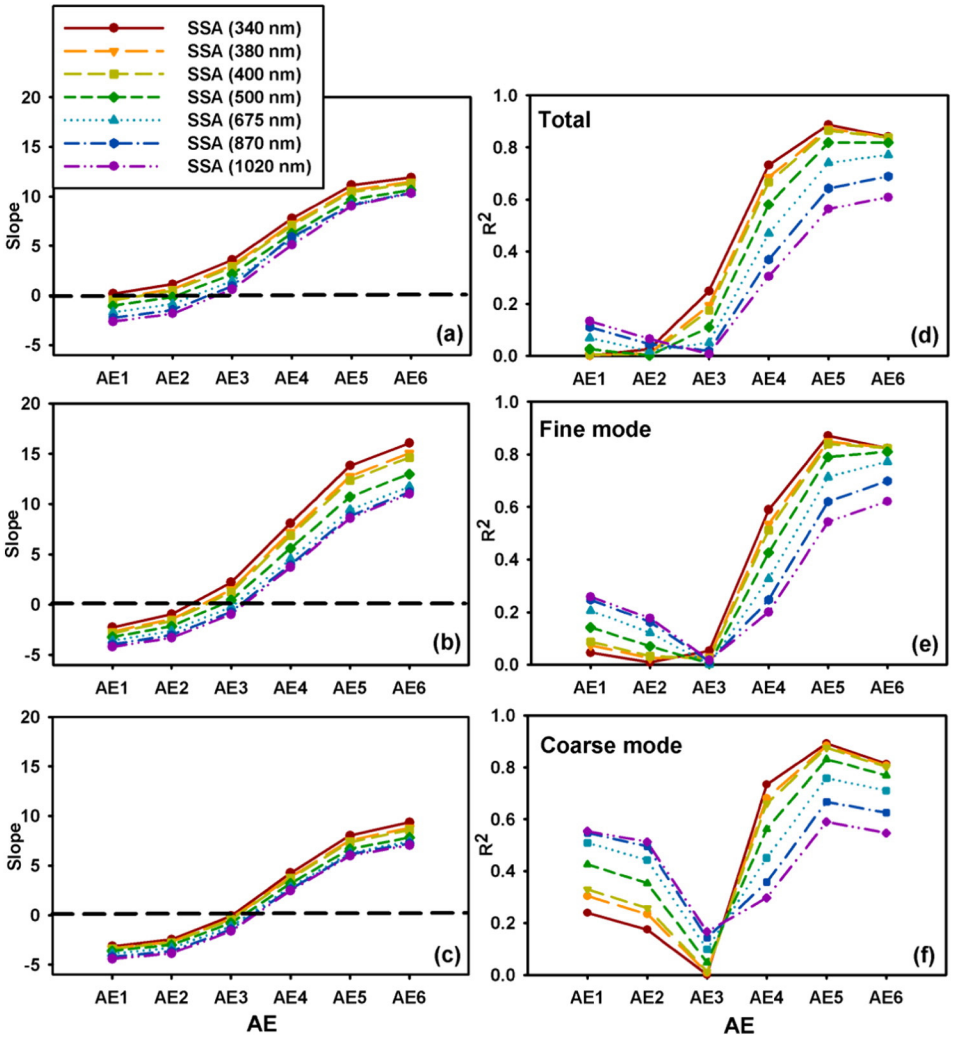

Fig. 2. Summary of correlations of single scattering albedo (SSA) at 7 different wavelengths such as 340 (red), 380 (orange), 400 (yellow green), 500 (green), 675 (cyan), 870 (blue), and 1020 nm (violet) with Ångström exponent (AE) at 6 wavelength pairs such as 340–380 (AE1), 380–400 (AE2), 400–500 (AE3), 500–675 (AE4), 675–870 (AE5), and 870–1020 (AE6) nm. Slopes of correlations for (a) total, (b) fine mode dominant, and (c) coarse mode dominant cases are shown on the left, and R^2 values of correlations for (d) total, (e) fine mode dominant, and (f) coarse mode dominant cases are shown on the right. (For interpretation of the references to color in this figure legend, the reader is referred to the web version of this article.)

known, AE represents the slope of linear correlation between AODs and wavelengths in a log scale (e.g., Eck et al., 1999). However, this relationship is not perfectly linear and actually expressed by the shape of the curvature. To explain this, previous studies used the derivative of AOD with respect to the wavelength in a logarithm scale, i.e., the second derivative of AE (Eck et al., 1999; Kaskaoutis and Kambezidis, 2006; Kedia and Ramachandran, 2009). Based on these studies, it was found that the shape of curvature in the wavelength-AOD plain of a logarithmic scale is convex up in the dominance of fine-mode aerosols such as biomass burning aerosols or urban aerosols, but convex down in the dominance of coarse-mode aerosols such as desert dust. Considering the extent of AEs (i.e., the slope of curvature) at the different wavelength pair, SW-AE is smaller than LW-AE in a convex-up curvature, but LW-AE is smaller than SW-AE in a convex-down curvature. Namely, large LW-AE and small SW-AE imply that the dominant atmospheric aerosol is fine mode, but small LW-AE and large SW-AE relate to the dominance of coarse mode particle in the regional atmosphere (see Supplement materials).

In brief, the fine and coarse mode cases can be divided by not only the AE in the visible wavelengths (400–675 nm), but also the wavelength dependence of AE between shorter and longer wavelengths. Then we compare these two different criteria based on Fig. 1. For the fine mode dominant case determined by the large AE (Fig. 1b), mostly SW-AEs are smaller than LW-AEs and this difference becomes more distinctive as SSA increases. For the coarse mode dominant case determined by the low AE (Fig. 1c), however, there are two different patterns; SW-AEs is larger than LW-AEs for low SSAs case but smaller for high SSA. This finding indicates that fine mode dominant case can be consistently distinguished by either AE or wavelength dependence of AE, while the coarse mode may not be clearly decided based on the AE, a typical criterion has been utilized. This feature will be more investigated in the next section.

Comparing SW-AEs to LW-AEs, correlations with SW-AEs are quite weaker than those of LW-AEs. Fig. 1 and Fig. 2 illustrate that the sensitivity of SW-AEs are relatively small compared to LW-AEs. Reid et al. (1999) showed the variation of SW-AE is not strongly influenced by the coarse-mode concentration while the variation of LW-AE is affected by the fine- and coarse-mode concentration equally. Schuster et al. (2006) found AE based on a 380–440 nm wavelength pair does not show strong correlation with fine mode volume fraction, as opposed to AE based on 670–870 nm. Based on these findings, it seems that LW-AE shows higher sensitivity to variation of particle size, resulting in the stronger correlation with SSA. LW-AE shows strong correlation with SSA in all three cases. If fine (AE at 400–675 nm > 0.75) and coarse mode (AE at 400–675 nm < 0.75) dominant cases are separately considered, weak correlations at SW-AE in total case (Fig. 1a) becomes

stronger in coarse mode dominant case. Again, this contrast comes from the reverse relationship of SW- and LW-AE between fine and coarse mode dominant cases. Additionally LW-AE shows stronger correlations with SW-SSA than with LW-SSA. Wavelength dependence of SSA seems associated with the mixing state of different aerosol types (Eck et al., 2010; Li et al., 2015), but why SW-SSA shows higher correlation is not yet interpreted. More investigation for this wavelength dependence of SSA seems necessary in the future to better understand the correlation pattern with AE.

Similar to our results, several studies also examined the difference of AEs according to the type of aerosols (Yang et al., 2009; Russell et al., 2010). They utilized the absorption AE and extinction (or scattering) AE estimated using SSA information, and suggested that desert dust shows larger absorbing AE but biomass burning and urban industrial aerosol shows larger extinction AE. Related to findings in this study, comparison of absorbing and extinction AE looks analogous to our analysis for the different correlations of SSA with SW-AE and LW-AE, respectively. If the wavelength dependence of AE can provide the information of aerosol types, it will be much beneficial because the SSA information should be obtained from the inversion method of the sky radiance (e.g., Estellés et al., 2012a), which is a relatively more uncertain and complicated process. In the next section we will more look into the ratio of AEs from the different wavelength pair to see the feasibility to use the wavelength dependence of AE for the regional aerosol classification.

3.2. The ratio between AE at shorter and longer wavelength pairs

In the previous section, correlations between SSAs and AEs were investigated in terms of the different wavelength dependence according to the dominant size and type of aerosol. This wavelength dependence of aerosol optical properties can also be applied for evaluating the spatiotemporal characteristics of regional aerosol (Ganguly et al., 2006). For example, the seasonal mean of SSAs at different channels and AEs at the different wavelength pairs may relate to the gap between the SW- and LW-AE (Supplementary materials). This relationship can be used to understand the variation of aerosol types. Thus, it is worthwhile to examine wavelength dependence of aerosol properties in this study, mainly for the characteristics of SW- and LW-AEs. Several previous studies have used the second derivative of AE to consider the wavelength dependence (Eck et al., 1999), and also examined the difference between SW- and LW-AE for the visualization of regional aerosol characteristics (Gobbi et al., 2007; Kedia and Ramachandran, 2009; Yoon et al., 2012; Zhu et al., 2016). To describe our findings easier, similarly we defined another index, AE ratio (AER), which is the ratio of LW-AE to SW-AE

$$\mathrm{AER} = \frac{\mathrm{LW-AE}}{\mathrm{SW-AE}} = \frac{\mathrm{AE(675-1020\ nm)}}{\mathrm{AE(340-675\ nm)}} \quad (1)$$

where two wavelength pairs of 340–675 and 675–1020 nm were selected to make similar range of wavelength in a logarithm scale for both SW-AE and LW-AE. Using this AER, the ratio of LW-AE to SW-AE, correlations between AER and SSA (500 nm) was first estimated for year 2006 and 2007 separately (Supplementary materials). Linear regression does not look weak but quadratic regression shows higher correlations (r^2) for both years. To understand this correlation shape, correlations between AER and SSA were divided based on AEs at 400–675 nm to consider the size of aerosol (Fig. 3). Interestingly, correlations between AER and SSA are clearly separated in accordance with the AE at 400–675 nm (Fig. 3). As the AE at 400–675 nm becomes large (fine mode dominance in general), AERs approach to 1.0–1.5 and SSA converges to around 0.95. This indicates that linear Angström relation under the dominance of small fine mode aerosols relates to the weak absorption property (Eck et al., 2001). In contrast, AER shows wide ranges as AE at 400–675 nm becomes small (approaching to the coarse

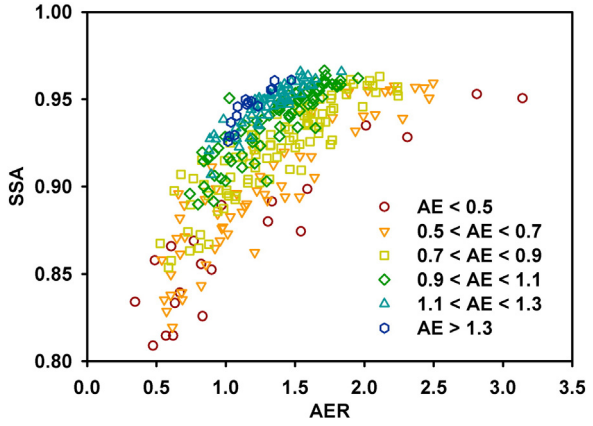

Fig. 3. Relationship between SSA at 500 nm and AER according to the 6 different cases of AE at 400–675 nm (expressed with different colors). (For interpretation of the references to color in this figure legend, the reader is referred to the web version of this article.)

mode dominance) and also the range of SSAs becomes broad. This large variation of AER and SSA in the coarse mode dominance illustrates that the wavelength dependence of aerosol properties occurs due to the different sensitivity of coarse mode aerosols according to the wavelength, similar to the idea in the previous section.

In Section 3.1, it was noticed that SW-AE is larger for the dominance of coarse mode aerosols such as desert dust and LW-AE is larger for the dominance of fine mode aerosols such as unban pollutants. Therefore, positive correlation between AER and SSA (Fig. 3) indicates that small AER is associated with the strong absorption properties of the dust particle (especially smaller than 1.0) and large AER relates to the weaker absorption properties of urban aerosols (especially larger than 2.0). These findings corroborate results of Russell et al. (2010), which connected absorbing AE to desert dust aerosols and extinction AE to biomass burning or urban aerosols.

Actually seasonal pattern of AER (Fig. 4) shows the same results as well. Considering the seasonal difference of the relationship between AER and SSA in Fig. 4a, broad range of correlations for small AE at 400–675 nm (i.e., AE at 400–675 nm < 0.75) can be divided into two seasons: spring (MAM) for small SSA and AER, and summer (JJA) for large AER and SSA. Also in the regime of small AE at 400–675 nm (coarse mode dominance), AER is smaller than 1.0 in spring (MAM), the main season of Asian dust occurrence, but larger than 2.0 in summer (JJA) showing strong urban pollution in general (Fig. 4b). In other words, the relationship of AER to SSA and AE reflects the seasonal variation of particle types. Different from the dust transported in spring, which is the obvious coarse mode particle, the properties of aerosols in summer are not clearly diagnosed. Based on Fig. 4, low AEs at 400–675 nm may not always indicate the real coarse-mode dominance if AER is higher than 1.0. Actually as AOD increases, sometimes LW-AE becomes larger than SW-AE (i.e., large AER) (Reid et al., 1999) and the radius of fine mode gradually increases (Dubovik et al., 2002; Zhu et al., 2016). Eck et al. (2012) also showed the existence of 'cloud-processed' aerosol with the larger radius in the fine mode. Thus, large AER may be resulted from the increase of the effective aerosol volume in the fine mode due to the severe pollution and loading, or particle growth by aging during the summertime in Seoul.

For extending the analysis between AER and SSA, finally AERs were compared to the SSAs of all seven wavelengths (Fig. 5). Regardless of wavelength, all SSAs show basically large correlations with AERs as confirmed in Fig. 3. Fig. 5 shows that SW-SSA (e.g., SSA at 340 nm) is lower for the AER smaller than 1.0 due to the strong absorption of shortwave radiation by dust aerosols but higher for the AER from 1.0 to 1.5 due to the strong scattering of shortwave radiation by urban aerosols. An interesting pattern appears with AER larger than 2.0, which is that SW-SSA is smaller again than LW-SSA (e.g., 1020 nm). Since AER larger than 2.0

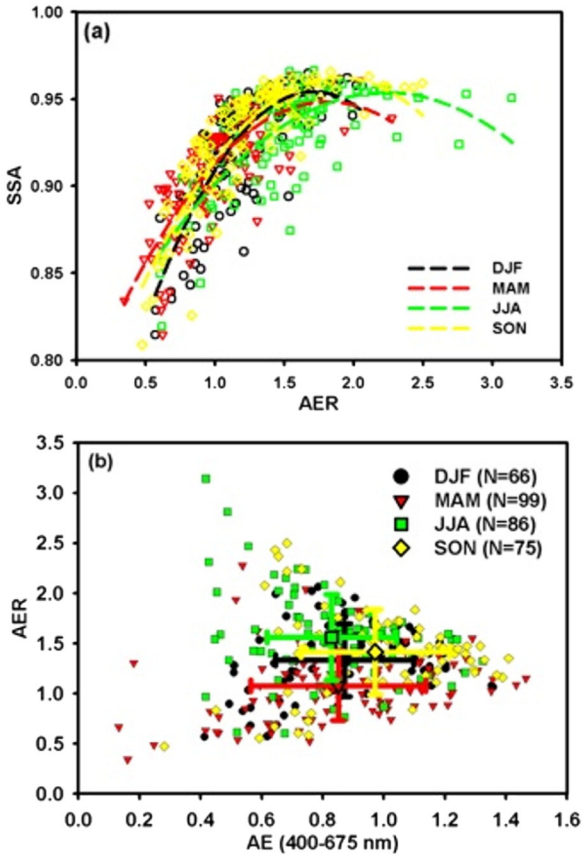

Fig. 4. Relationship of AE at 400–675 nm to (a) SSA at 500 nm and (b) AER according to the 4 different seasons, which are DJF (winter, black), MAM (spring, red), JJA (summer, green), and SON (autumn, yellow). Dashed lines are quadratic fitting lines and cross bars show the range of 1-σ standard deviation. (For interpretation of the references to color in this figure legend, the reader is referred to the web version of this article.)

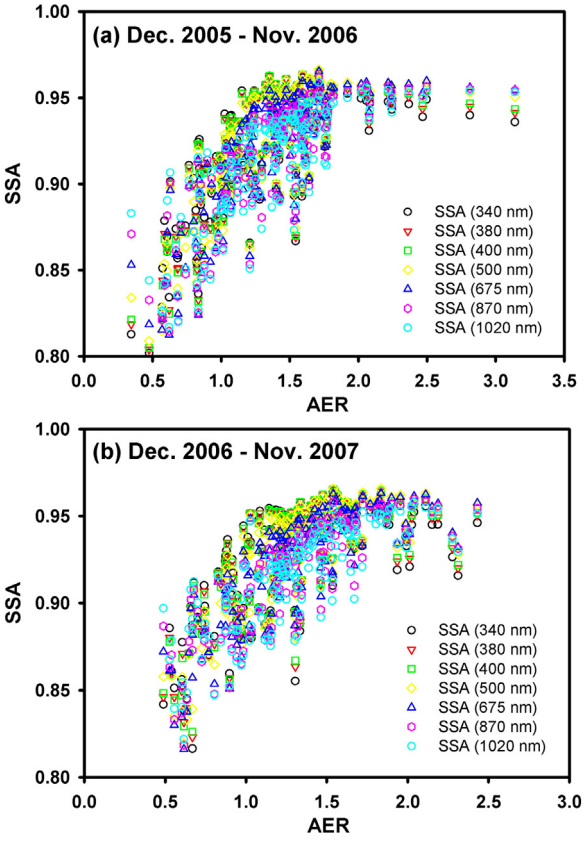

Fig. 5. Relationship between AER and SSA at 7 different wavelengths such as 340 (black), 380 (red), 400 (green), 500 (yellow), 675 (blue), 870 (pink), and 1020 nm (cyan) for the period from (a) December 2005 to November 2006, and (b) December 2006 to November 2007. (For interpretation of the references to color in this figure legend, the reader is referred to the web version of this article.)

relates to the urban aerosol in summer as discussed in Fig. 4, SSA should be larger in the short wavelength based on previous studies showing the higher SSA in the short wavelength under the urban polluted areas (Dubovik et al., 2002; Russell et al., 2010).

To figure out this new feature, we also examine the difference between SSA at 340 nm (the shortest wavelength) and SSA at 1020 nm (the longest wavelength) in Fig. 6. This SSA difference is sometimes negative not only in spring but also in summer for both year 2006 and 2007. Since iron oxides in mineral dust aerosol have short wavelength absorption (Sokolik and Toon, 1999; Derimian et al., 2008), the exhibited spectral dependence in spring is due to the effect of dust events. But the feature in summer (i.e., SW-SSA < LW-SSA for large AER) is different from what we expect, implying that the possibility to detect another aerosol type during the summertime at Seoul. Actually the annual pattern of back-trajectories at Seoul indicates that the summertime air mass is not attributed to the dust transport from the China or Mongolia desert regions (Koo, 2008).

Therefore, it is necessary to understand which kind of aerosol may contribute to the strong shortwave absorbing (small SW-SSA) in summer. One possibility is the glyoxal taken by the aerosol in the heterogeneous phase. Glyoxal has the substantial absorption at 300 to 400 nm (Shapiro et al., 2009) and it shows a significant portion in organic aerosols (Volkamer et al., 2007). Even though satellite measurements showed that the maximum peak of glyoxal in East Asia occurs in July and August (Vrekoussis et al., 2009), however, the amount of glyoxal does not seem abundant to influence the local characteristics of radiative absorption.

We presume that the summertime shortwave absorption property may be attributed to the brown carbon, which is the representative aerosol having strong absorption between 300 and 400 nm range (Andreae and Gelencsér, 2006). Hecobian et al. (2010) showed the enhancement of absorption coefficients at 365 nm during the

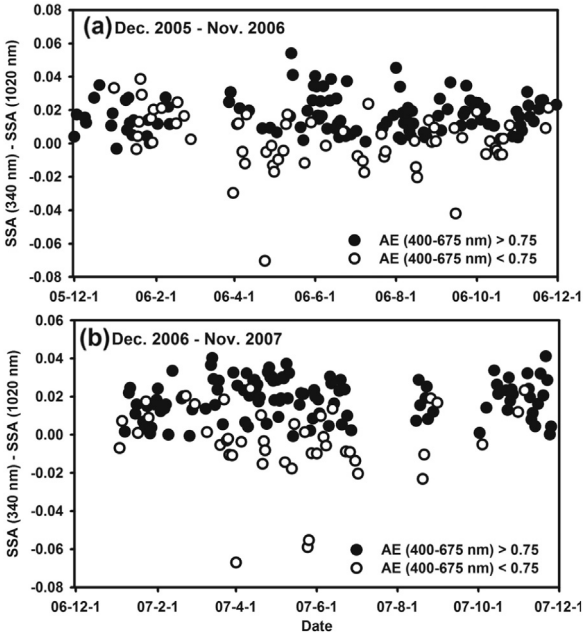

Fig. 6. Time series of the difference between SSA at 340 nm and SSA at 1020 nm for the period from (a) December 2005 to November 2006, and (b) December 2006 to November 2007.

summertime in Atlanta, United States, especially in the afternoon. They explained that this shortwave absorption is due to the conversion of water soluble organic carbon to more light-absorbing compounds, or partitioning of more efficient light absorbing semi-volatile organic carbons to the aerosol. In the summertime afternoon of Los Angeles, the shortwave absorption is 3 times higher than that in Atlanta (Zhang et al., 2011) revealing that the hygroscopic feature of brown carbon enhances the shortwave absorption much. These in-situ results are also consistent with the feasible hygroscopic growth of particle with small AE in polluted conditions (Eck et al., 2012), and UV-visible light absorption by the brown carbon species in the summertime cloud water (Desyaterik et al., 2013). Summarizing these findings in the polluted area, negative difference of SSA between 340 and 1020 nm during summer probably shows the enhancement of shortwave absorption due to the increase of soluble brown carbon at Seoul. This means that wavelength dependence of aerosol properties obtained from skyradiometer observations can provide the information even for the secondary organic aerosol. More intensive study with optical and chemical instrumentation will be required in the future for the validation of this idea.

4. Summary and conclusion

In this study, the wavelength dependence of SSA and AE was investigated for the analysis of size and type of aerosol at Seoul. The correlation between SSAs and AEs basically shows the scattering pattern of fine mode and absorbing pattern of coarse mode particle in the region. However, correlations of SSAs are stronger with LW-AEs than SW-AEs because LW-AE shows larger sensitivity to the particle size. The wavelength dependence of SSA also exists and changes the extent of correlations with AEs. Analysis for the relationship between SSA and AE in the multiple wavelength seems useful to be utilized for figuring out the relative optical influence of both fine- and coarse-mode aerosols.

For further investigation about the wavelength dependence, AER is considered. AER shows large variation if AE at 400–675 nm is small, and SSAs also follows this large variation, showing that the small AE at 400–675 nm does not always indicate the coarse mode dominant condition. Based on the seasonal pattern of AER and the comparison to SSA at different wavelengths, it seems that AER smaller than 1.0 implies the coarse-mode dust aerosol and AER between 1.0 and 2.0 means the fine mode aerosol with large scattering. It is not clear which aerosol corresponds to the AER larger than 2.0, but the peculiar pattern in summer implies that some of secondary organic aerosol such as brown carbon can be associated with this regime of AER.

This study shows the possibility of improving aerosol classification based on the wavelength dependence of aerosol. Previously, several algorithms for the aerosol classification were devised using the aerosol optical properties such as AE, SSA, and fine mode fraction. But this study shows that SSA or AE near the 500 nm (usually used in the retrieval algorithm of aerosol classification) themselves does not perfectly identify the size and composition of aerosol in the coarse-mode dominant area. We expect that the application of wavelength dependence enables better aerosol classification and possibly provides more accurate information of regional radiative forcing.

Acknowledgements

This study was supported by the Korea Polar Research Institute (KOPRI, PE16090).

Appendix A. Supplementary data

Supplementary data to this article can be found online at http://dx.doi.org/10.1016/j.atmosres.2016.06.006.

References

Alam, K., Trautmann, T., Blaschke, T., 2011. Aerosol optical properties and radiative forcing over mega-city Karachi. Atmos. Res. 101, 773–782.
Andreae, M.O., Gelencsér, A., 2006. Black carbon or brown carbon? The nature of light-absorbing carbonaceous aerosols. Atmos. Chem. Phys. 6, 3131–3148.
Aoki, K., Fujiyoshi, Y., 2003. Sky radiometer measurements of aerosol optical properties over Sapporo, Japan. J. Meteorol. Soc. Jpn. 81, 493–513.
Boi, P., Tonna, G., Dalu, G., Nakajima, T., Olivieri, B., Pompei, A., Campanelli, M., Rao, R., 1999. Calibration and data elaboration procedure for sky irradiance measurements. Appl. Opt. 38, 896–907.
Cachorro, V.E., de Frutos, A.M., Casanova, J.L., 1987. Determination of the Angstrom turbidity parameters. Appl. Opt. 26, 3069–3076.
Charson, R.J., Schwarts, S.E., Hales, J.M., Cess, R.D., Coakley, J.A., Hansen Jr., J.E., Hofmann, D.J., 1992. Climate forcing by anthropogenic aerosols. Science 255, 423–430.
Che, H., Shi, G., Uchiyama, A., Yamazaki, A., Chen, H., Goloub, P., Zhang, X., 2008. Intercomparison between aerosol optical properties by a PREDE skyradiometer and CIMEL sunphotometer over Beijing, China. Atmos. Chem. Phys. 8, 3199–3214.
Cheymol, A., Gonzalex Sotelino, L., Lam, K.S., Kim, J., Fioletov, V., Siani, A.M., De Backer, H., 2009. Intercomparison of aerosol optical depth from Brewer ozone spectrophotometers and CIMEL sunphotometers measurements. Atmos. Chem. Phys. 9, 733–741.
Cho, H.K., 1980. On the size distribution of atmospheric aerosol particles from spectral photometric measurement in Seoul. J. Kor. Meteorol. Soc. 16, 175–183.
Cho, H.-K., 1981. The variation of atmospheric turbidity over Seoul. J. Kor. Meteorol. Soc. 17, 208–228.
Cho, H.M., Lee, S.-M., Cho, H.-K., 1984. The characteristics of the aerosol optical depth in the visible region. J. Kor. Meteorol. Soc. 20, 302–309.
Cho, H.K., Jeong, M.J., Kim, J., Kim, Y.J., 2003. Dependence of diffuse photosynthetically active solar irradiance on total optical depth. J. Geophys. Res. 108, 4267.
De Bock, V., De Backer, H., Mangold, A., Delcloo, A., 2010. Aerosol optical depth measurements at 340 nm with a Brewer spectrophotometer and comparison with Cimel sunphotometer observations at Uccle, Belgium. Atmos. Meas. Tech. 3, 1577–1588.
Derimian, Y., Léon, J.-F., Dubovik, O., Chapello, I., Tanré, D., Sinyuk, A., Auriol, F., Podvin, T., Brogniez, G., Holben, B.N., 2008. Radiative properties of aerosol mixture observed during the dry season 2006 over M'Bour, Senegal (African Monsoon Multidisciplinary Analysis campaign). J. Geophys. Res. 113, D00C09.
Desyaterik, Y., Sun, Y., Shen, X., Lee, T., Wang, X., Wang, T., Collett Jr., J.L., 2013. Speciation of "brown" carbon in cloud water impacted by agricultural biomass burning in eastern China. J. Geophys. Res. 118, 7389–7399.
Dubovik, O., Holben, B.N., Kaufman, Y.J., Yamasoe, M., Smirnov, A., Tanré, D., Slutsker, I., 1998. Single-scattering albedo of smoke retrieved from the sky radiance and solar transmittance measured from ground. J. Geophys. Res. 103, 31903–31923.
Dubovik, O., Holben, B., Eck, T.F., Smirnov, A., Kaufman, Y.J., King, M.D., Tanré, D., Slutsker, I., 2002. Variability of absorption and optical properties of key aerosol types observed in worldwide locations. J. Atmos. Sci. 59, 590–608.
Eck, T.F., Holben, B.N., Reid, J.S., Dubovik, O., Smirnov, A., O'Neill, N.T., Slutsker, I., Kinne, S., 1999. Wavelength dependence of the optical depth of biomass burning, urban, and desert dust aerosols. J. Geophys. Res. 104, 31333–31349.
Eck, T.F., Holben, B.N., Ward, D.E., Dubovik, O., Reid, J.S., Smirnov, A., Mukelabai, M.M., Hsu, N.C., O'Neill, N.T., Slutsker, I., 2001. Characterization of the optical properties of biomass burning aerosol in Zambia during the 1997 ZIBBEE field campaign. J. Geophys. Res. 106, 3425–3448.
Eck, T.F., Holben, B.N., Reid, J.S., O'Neill, N.T., Schafer, J.S., Dubovik, O., Smirnov, A., Yamasoe, M.A., Artaxo, P., 2003. High aerosol optical depth biomass burning events: a comparison of optical properties for different source regions. Geophys. Res. Lett. 30, 2035.
Eck, T.F., Holben, B.N., Dubovik, O., Smirnov, A., Goloub, P., Chen, H.B., Chatenet, B., Gomes, L., Zhang, X.-Y., Tsay, S.-C., Ji, Q., Giles, D., Slutsker, I., 2005. Columnar aerosol optical properties at AERONET sites in central eastern Asia and aerosol transport to the tropical mid-Pacific. J. Geophys. Res. 110, D06202.
Eck, T.F., Holben, B.N., Reid, J.S., Sinyuk, A., Dubovik, O., Smirnov, A., Giles, D., O'Neill, N.T., Tsay, S.-C., Ji, Q., Al Mandoos, A., Ramzan Khan, M., Reid, E.A., Schafer, J.S., Sorokine, M., Newcomb, W., Slutsker, I., 2008. Spatial and temporal variability of column-integrated aerosol optical properties in the southern Arabian Gulf and United Arab Emirates in summer. J. Geophys. Res. 113, D01204.
Eck, T.F., Holben, B.N., Sinyuk, A., Pinker, R.T., Goloub, P., Chen, H., Chatenet, B., Li, Z., Singh, R.P., Tripathi, S.N., Reid, J.S., Giles, D.M., Dubovik, O., O'Neill, N.T., Smirnov, A., Wang, P., Xia, X., 2010. Climatological aspects of the optical properties of fine/coarse mode aerosol mixtures. J. Geophys. Res. 115, D19205.
Eck, T.F., Holben, B.N., Reid, J.S., Giles, D.M., Rivas, M.A., Singh, R.P., Tripathi, S.N., Bruegge, C.J., Platnick, S., Arnold, G.T., Krotkov, N.A., Carn, S.A., Sinyuk, A., Dubovik, O., Arola, A., Schafer, J.S., Artaxo, P., Smirnov, A., Chen, H., Goloub, P., 2012. Fog- and cloud-induced aerosol modification observed by the Aerosol Robotic Network (AERONET). J. Geophys. Res. 117, D07206.
El-Metwally, M., Alfaro, S.C., 2013. Correlation between meteorological conditions and aerosol characteristics at an East-Mediterranean coastal site. Atmos. Res. 132-133, 76–90.
Estellés, V., Campanelli, M., Utrillas, M.P., Expósito, F., Martínez-Lozano, J.A., 2012a. Comparison of AERONET and SKYRAD4.2 inversion products retrieved from a Cimel CE318 sunphotometer. Atmos. Meas. Tech. 5, 569–579.
Estellés, V., Campanelli, M., Smyth, T.J., Utrillas, M.P., Martínez-Lozano, J.A., 2012b. Evaluation of the new ESR network software for the retrieval of direct sun products from CIMEL CE318 and PREDE POM01 sun-sky radiometers. Atmos. Chem. Phys. 12, 11619–11630.
Ganguly, D., Jayaraman, A., Gadhavi, H., 2006. Physical and optical properties of aerosols over an urban location in western India: seasonal variabilities. J. Geophys. Res. 111, D24206.

Gobbi, G.P., Kaufman, Y.J., Koren, I., Eck, T.F., 2007. Classification of aerosol properties derived from AERONET direct sun data. Atmos. Chem. Phys. 7, 453–458.
Guo, J., Zhang, X., Cao, C., Che, H., Liu, H., Gupta, P., Zhang, H., Xu, M., Li, X., 2010. Monitoring haze episodes over the Yellow Sea by combining multisensory measurements. Int. J. Remote Sens. 31, 4743–4755.
Hecobian, A., Zhang, X., Zheng, M., Frank, N., Edgerton, E.S., Weber, R.J., 2010. Water-soluble organic aerosol material and the light-absorption characteristics of aqueous extracts measured over the southeastern United States. Atmos. Chem. Phys. 10, 5965–5977.
Holben, B.N., Eck, T.F., Slutsker, I., Tanré, D., Buis, J.P., Setzer, A., Vermote, E., Raegan, J.A., Kaufman, Y.J., Nakajima, T., Lavenu, F., Jankowiak, I., Smirnov, A., 1998. AERONET - a federated instrument network and data archive for aerosol characterization. Remote Sens. Environ. 66, 1–16.
Huang, J., Guo, J., Wang, F., Liu, Z., Jeong, M.-J., Yu, H., Zhang, Z., 2015. CALIPSO inferred most probable heights of global dust and smoke layers. J. Geophys. Res. 120, 5085–5100.
IPCC, Climate Change 2013, 2013. The Physical Science Basis, the Working Group I Contribution to the UN IPCC's Fifth Assessment Report (WG1 AR5). Cambridge University Press, New York, U.S.A, pp. 159–254.
Kaskaoutis, D.G., Kambezidis, H.D., 2006. Investigation into the wavelength dependence of the aerosol optical depth in the Athens area. Q. J. R. Meteorol. Soc. 132, 2217–2234.
Kaufman, Y.J., 1993. Aerosol optical thickness and atmospheric path radiance. J. Geophys. Res. 98, 2677–2692.
Kedia, S., Ramachandran, S., 2009. Variability in aerosol optical and physical characteristics over the Bay of Bengal and the Arabian Sea deduced from Ångström exponents. J. Geophys. Res. 114, D14207.
Kerr, J.B., 2002. New methodology for deriving total ozone and other atmospheric variables from Brewer spectrophotometer direct sun spectra. J. Geophys. Res. 107, 4731.
Khatri, P., Takamura, T., 2009. An algorithm to screen cloud-affected data for sky radiometer data analysis. J. Meteorol. Soc. Jpn. 87, 189–204.
Kim, K.W., He, Z., Kim, Y.J., 2004a. Physicochemical characteristics and radiative properties of Asian dust particles observed at Kwangju, Korea, during the 2001 ACE-Asia intensive observation period. J. Geophys. Res. 109, D19S02.
Kim, D.-H., Sohn, B.-J., Nakajima, T., Takemura, T., Takemura, T., Choi, B.-C., Yoon, S.-C., 2004b. Aerosol optical properties over east Asia determined from ground-based sky radiation measurements. J. Geophys. Res. 109, D02209.
Kim, D.-H., Sohn, B.-J., Nakajima, T., Takemura, T., 2005. Aerosol radiative forcing over east Asia determined from ground-based solar radiation measurements. J. Geophys. Res. 110, D10S22.
Kim, J., Lee, J., Lee, H.C., Higurashi, A., Takemura, T., Song, C.H., 2007a. Consistency of the aerosol type classification from satellite remote sensing during the Atmospheric Brown Cloud – East Asia Regional Experiment campaign. J. Geophys. Res. 112, D22S33.
Kim, S.W., Yoon, S.-C., Kim, J., Kim, S.-Y., 2007b. Seasonal and monthly variations of columnar aerosol optical properties over East Asia determined from multi-year MODIS, LIDAR, and AERONET sun/sky radiometer measurements. Atmos. Environ. 41, 1634–1651.
Koo, J.-H., 2008. Optical Properties of Aerosol in a Megacity, Seoul From Ground-based and Satellite Measurements (M.S. thesis) Dept. of Atmospheric Sciences, The Yonsei University.
Lee, K.H., Li, Z., Wong, M.S., Xin, J., Wang, Y., Hao, W.-M., Zhao, F., 2007. Aerosol single scattering albedo estimated across China from a combination of ground and satellite measurements. J. Geophys. Res. 112, D22S15.
Lee, J., Kim, J., Song, C.H., Ryu, J.-H., Ahn, Y.-H., Song, C.K., 2010a. Algorithm for retrieval of aerosol optical properties over the ocean from the Geostationary Ocean Color Imager. Remote Sens. Environ. 114, 1077–1088.
Lee, J., Kim, J., Song, C.H., Kim, S.B., Chun, Y.S., Sohn, B.J., Holben, B.N., 2010b. Characteristics of aerosol types from AERONET sunphotometer measurements. Atmos. Environ. 44, 3110–3117.
Li, J., Carlson, B.E., Lacis, A.A., 2015. Using single-scattering albedo spectral curvature to characterize East Asian aerosol mixtures. J. Geophys. Res. 120, 2037–2052.
Liou, K.N., 2002. An Introduction to Atmospheric Radiation: 2nd Edition. Academic Press.
Liu, J., Zheng, Y., Li, Z., Wu, R., 2008. Ground-based remote sensing of aerosol optical properties in one city in Northwest China. Atmos. Res. 89, 194–205.
Masmoudi, M., Alfaro, S.C., El Metwally, M., 2015. A comparison of the physical properties of desert dust retrieved from the sunphotometer observation of major events in the Sahara, Sahel, and ArabianPeninsula. Atmos. Res. 158-159, 24–35.
Nakajima, T., Tonna, G., Rao, R., Boi, P., Kaufman, Y., Holben, B., 1996. Use of sky brightness measurements from ground for remote sensing of particulate polydispersions. Appl. Opt. 35, 2672–2686.
Ningombam, S.S., Bagare, S.P., Sinha, N., Singh, R.B., Srivastava, A.K., Larson, E., Kanawade, V.P., 2014. Characterization of aerosol optical properties over the high-altitude station Hanle, in the trans-Himalayan region. Atmos. Res. 138, 308–323.
Ningombam, S.S., Bagare, S.P., Khatri, P., Sohn, B.J., Song, H.-J., 2015. Estimation of aerosol radiative forcing over an aged-background aerosol feature during advection and non-advection events using a ground-based data obtained from a Prede Skyradiometer observation. Atmos. Res. 164-165, 76–83.
Reid, J.S., Eck, T.F., Christopher, S.A., Hobbs, P.V., Holben, B., 1999. Use of Ångstrom exponent to estimate the variability of optical and physical properties of aging smoke particle in Brazil. J. Geophys. Res. 104, 27473–27489.
Rosenfeld, D., 2000. Suppression of rain and snow by urban and industrial air pollution. Science 287, 1793–1796.
Russell, P.B., Bergstrom, R.W., Shinozuka, Y., Clarke, A.D., DeCarlo, P.F., Jimenez, J.L., Livingston, J.M., Redemann, J., Dubovik, O., Strawa, A., 2010. Absorption Angtrom exponent in AERONET and related data as an indicator of aerosol composition. Atmos. Chem. Phys. 10, 1155–1169.
Schuster, G.L., Dubovik, O., Holben, B.N., 2006. Angstrom exponent and bimodal size distributions. J. Geophys. Res. 111, D07207.
Shapiro, E.L., Szprengiel, J., Sareen, N., Jen, C.N., Giordano, M.R., McNeill, V.F., 2009. Light-absorbing secondary organic material formed by glyoxal in aqueous aerosol mimics. Atmos. Chem. Phys. 9, 2289–2300.
Smirnov, A., Holben, B.N., Eck, T.F., Dubovik, O., Slutsker, I., 2000. Cloud-screening and quality control algorithms for the AERONET database. Remote Sens. Environ. 73, 337–349.
Sokolik, I.N., Toon, O.B., 1999. Incorporation of mineralogical composition into models of the radiative properties of mineral aerosol from UV to IR wavelengths. J. Geophys. Res. 104, 9423–9444.
Song, H.-J., Sohn, B.-J., Chun, H.-W., Chun, Y., Lee, S.-S., 2014. Improved cloud screening method for the analysis of sky radiometer measurements and application to Asian dust detection. J. Meteorol. Soc. Jpn. 92A, 167–183.
Takamura, T., Nakajima, T., 2004. Overview of SKYNET and its activities. Opt. Pura Apl. 37, 3303–3308.
Volkamer, R., San Martini, F., Molina, L.T., Salcedo, D., Jimenez, J.L., Molina, M.J., 2007. A missing sink for gas-phase glyoxal in Mexico City: formation of secondary organic aerosol. Geophys. Res. Lett. 34, L19807.
Vrekoussis, M., Wittrock, F., Richter, A., Burrows, J.P., 2009. Temporal and spatial variability of glyoxal as observed from space. Atmos. Chem. Phys. 9, 4485–4504.
Wang, Y., Xin, J., Li, Z., Wang, S., Wang, P., Hao, W.M., Nordgren, B.L., Chen, H., Wang, L., Sun, Y., 2011. Seasonal variations in aerosol optical properties over China. J. Geophys. Res. 116, D18209.
Xin, J., Wang, Y., Li, Z., Wang, P., Hao, W.M., Nordgren, B.L., Wang, S., Liu, G., Wang, L., Wen, T., Sun, Y., Hu, B., 2007. Aerosol optical depth (AOD) and Ångström exponent of aerosols observed by the Chinese Sun Hazemeter Network from August 2004 to September 2005. J. Geophys. Res. 112, D05203.
Yang, M., Howell, S.G., Zhuang, J., Huebert, B.J., 2009. Attribution of aerosol light absorption to black carbon, brown carbon, and dust in China – interpretations of atmospheric measurements during EAST-AIRE. Atmos. Chem. Phys. 9, 2035–2050.
Yoon, J., von Hoyningen-Huene, W., Kokhanovsky, A.A., Burrows, J.P., 2012. Trend analysis of aerosol optical thickness and Ångström exponent derived from the global AERONET spectral observations. Atmos. Meas. Tech. 5, 1271–1299.
Zhang, X., Lin, Y.-H., Surratt, J.D., Zotter, P., Prévôt, A.S.H., Weber, R.J., 2011. Light-absorbing soluble organic aerosol in Los Angeles and Atlanta: a contrast in secondary organic aerosol. Geophys. Res. Lett. 38, L21810.
Zhu, J., Xia, X., Che, H., Wang, J., Zhang, J., Duan, Y., 2016. Study of aerosol optical properties at Kunming in southwest China and long-range transport of biomass burning aerosols from North Burma. Atmos. Res. 169, 237–247.